Supporting Information

Scaffold-Reinforced Perovskite Compound Solar Cells

Brian L. Watson[1,†], Nicholas Rolston[2,†], Adam D. Printz[1,†], and Reinhold H. Dauskardt[1,*]

[1]Department of Materials Science and Engineering, Stanford University, Stanford, CA, 94305-2205, USA

[2]Department of Applied Physics, Stanford University, Stanford, CA, 94305-4090, USA

[†]Equal contributions

*Author to whom correspondence should be addressed: dauskardt@stanford.edu

Contents

1. Optical micrographs of scaffolds

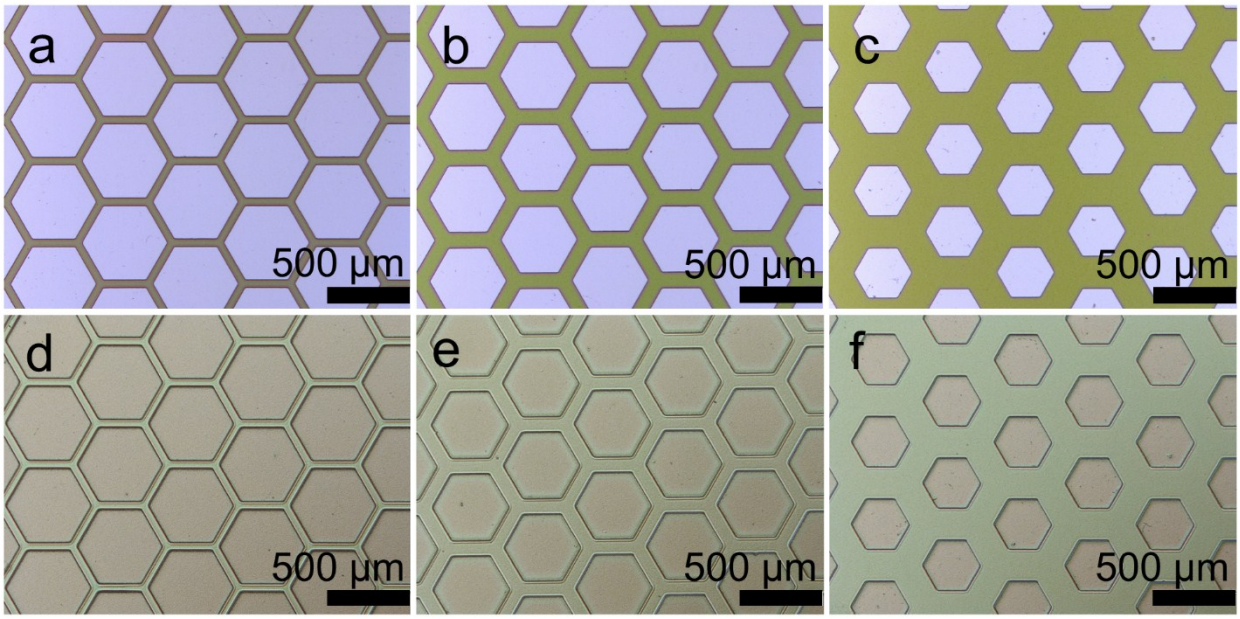

Figure S1. Optical micrographs of unfilled scaffolds (green) on Si and TiO_2 (blue) with different wall widths: (a) 50 µm, (b) 100 µm, and (c) 200 µm. Optical micrographs of scaffolds filled with perovskite: (d) 50 µm, (e) 100 µm, and (f) 200 µm scaffold wall widths.

2. Profilometry line-scans and images of DCB fracture surfaces filled scaffolds

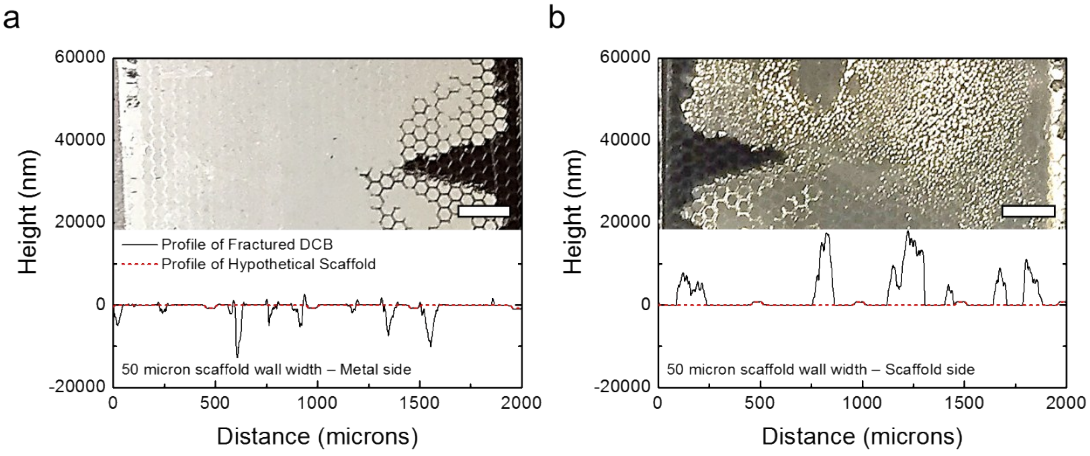

Figure S2. Profilometry line-scans of the 50 µm scaffold DCB after fracture (a) on the metal side and (b) on the scaffold side. The red dashed line is an approximation of where the scaffolds should be in the line-scans. Insets: photographs of the scaffold beams after fracture. On the metal side, the white regions are failure through the epoxy or at the epoxy/metal interface. On the scaffold side, the gray region also indicates failure through the epoxy and at the epoxy/metal interface. The darker regions on both sides of the specimen are failure in the perovskite. Scale bars are 2 mm.

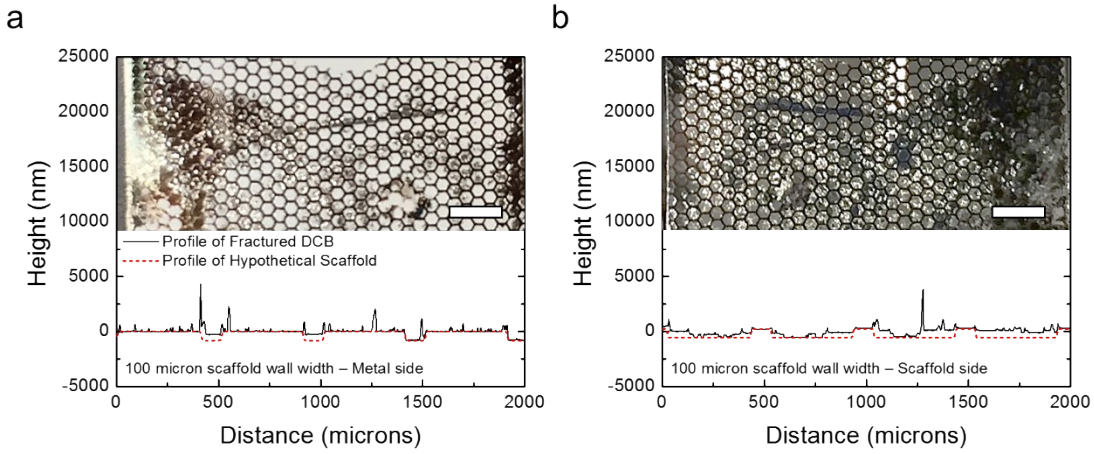

Figure S3. Profilometry line-scans of the 100 µm scaffold DCB after fracture (a) on the metal side and (b) on the scaffold side. The red dashed line is an approximation of where the scaffolds should be in the line-scans. Some scaffold fracture is evident on the metal side of the beam. Insets: photographs of the scaffold beams after fracture. The white/gray regions are fracture through the epoxy, while the dark regions indicate fracture through the perovskite. Scale bars are 2 mm.

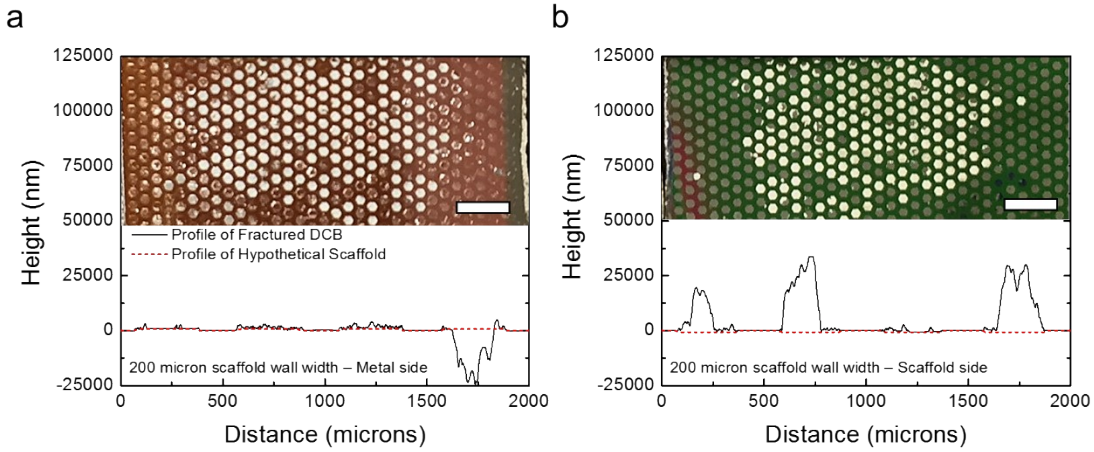

Figure S4. Profilometry line-scans of the 200 µm scaffold DCB after fracture (a) on the metal side and (b) on the scaffold side. The red dashed line is an approximation of where the scaffolds should be in the line-scans. Insets: photographs of the scaffold beams after fracture. The white regions are failure through the epoxy. The other regions are failure in the perovskite and the PTAA/scaffold interface. Scale bars are 2 mm.

3. XPS spectra of fracture surfaces

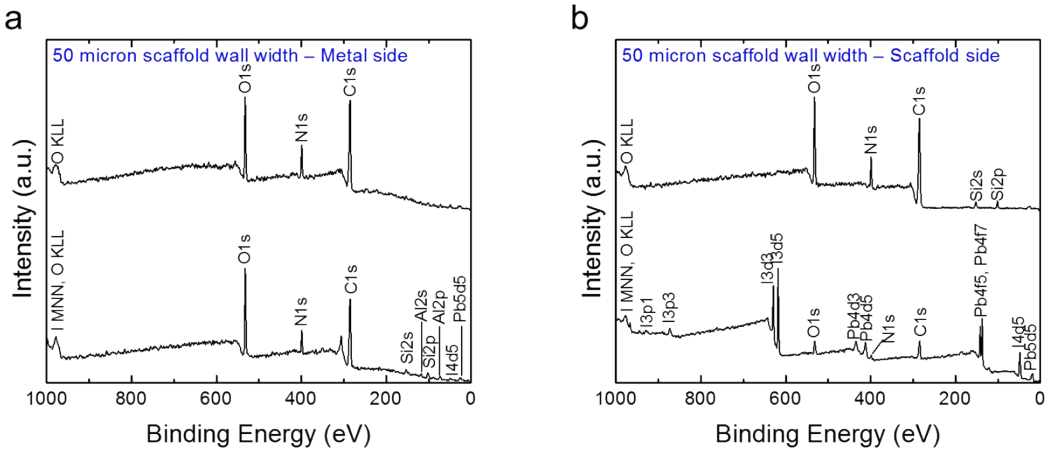

Figure S5. XPS spectra of taken at different regions of the 50 µm scaffold wall width DCB after fracture (a) on the metal side and (b) on the scaffold side. The low intensity of the Pb and I peaks on the metal side indicate that the fracture path generally avoided the perovskite, while the relatively high intensity C, N, and O peaks suggest that the fracture was through the encapsulating layers. The spectra on the scaffold side suggests a fracture path that meandered through the entire test structure.

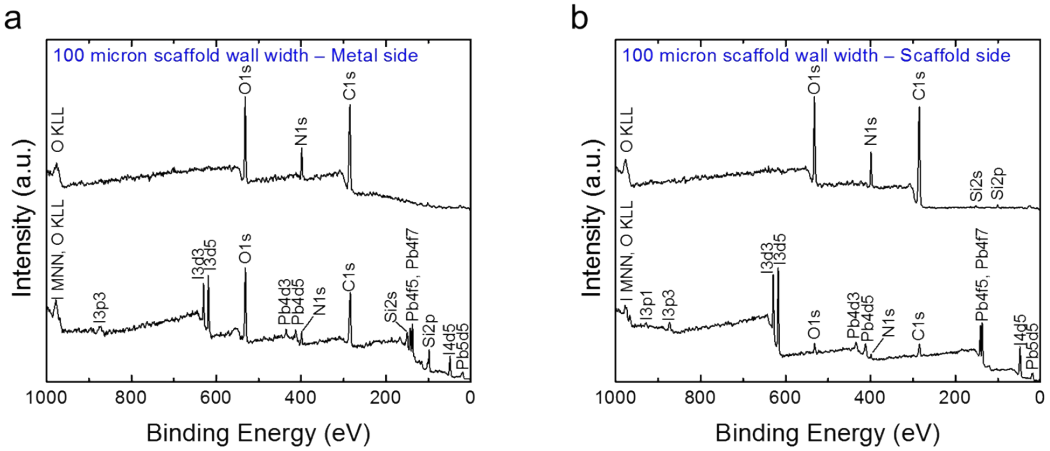

Figure S6. XPS spectra of taken at different regions of the 100 µm scaffold wall width DCB after fracture (a) on the metal side and (b) on the scaffold side. The spectra indicate a fracture path that meandered through the test structure, fracturing both through the epoxy (top line scans) and through the perovskite (bottom line scans).

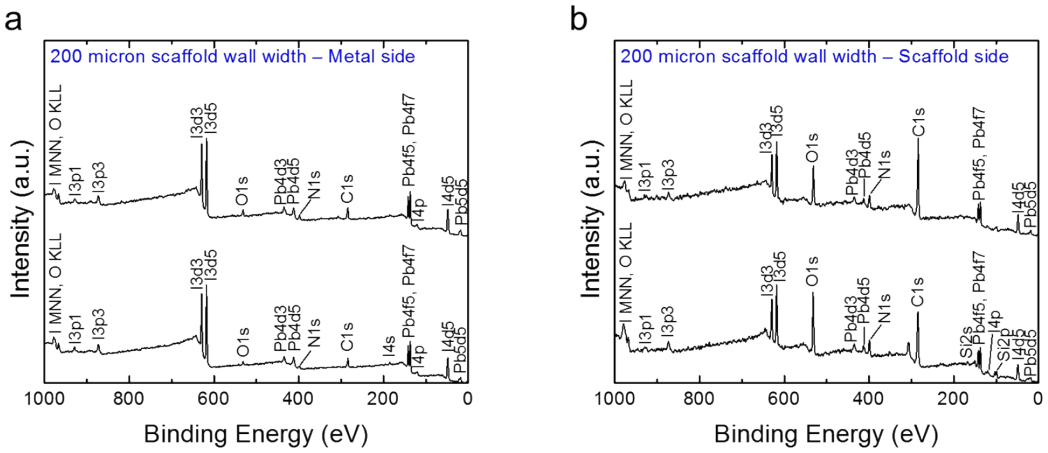

Figure S7. XPS spectra of taken at different regions of the 200 µm scaffold wall width DCB after fracture (a) on the metal side and (b) on the scaffold side. While profilometry showed a fracture path that meandered through the test structure, the Pb and I peaks on both the metal and scaffold side XPS spectra suggest that the fracture path frequently propagated through the perovskite.

4. Averaged *J-V* curves of solar cells

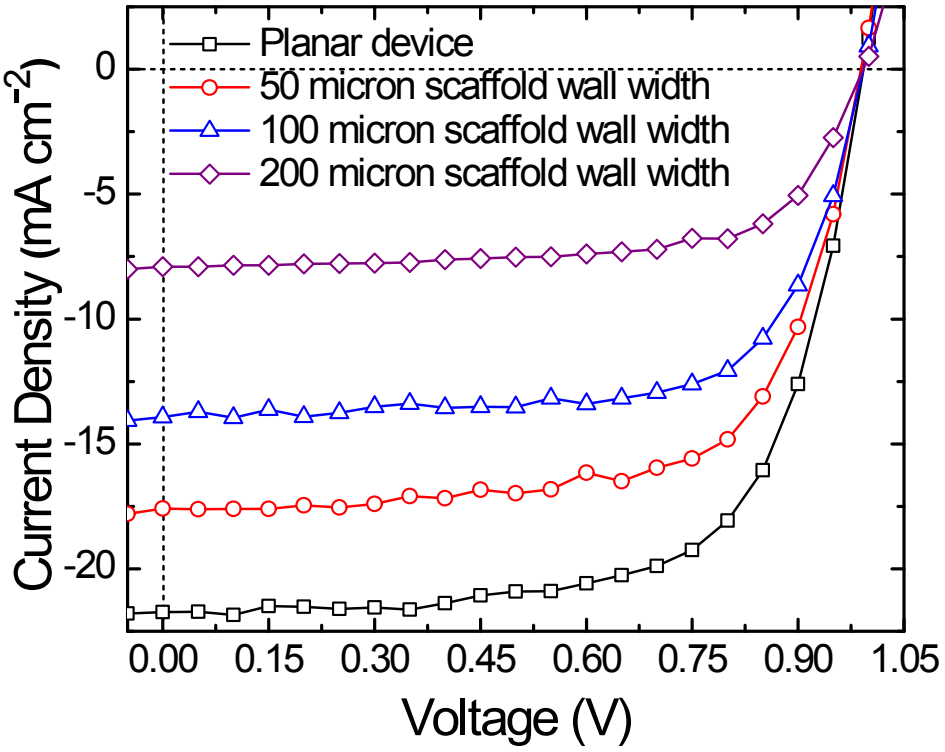

Figure S8. Averaged *J-V* curves of devices with the architecture ITO/TiO_2 NPs/C_{60}/$CH_3NH_3PbI_3$/PTAA/Ag and scaffold wall widths of 50 µm, 100 µm, and 200 µm per 500 µm period (as well as scaffold-free planar devices).

5. Hysteresis of solar cells

Table S1. *PCE* values for backward and forward *J-V* scans, showing minimal relative hysteresis of less than a 10% difference in magnitude based on the scan direction.

Solar Cell Type	Backward *PCE* (%)	Forward *PCE* (%)	Relative Hysteresis (%)
Planar	15.4	13.9	9.1
50 µm scaffold wall width	12.2	11.7	4.1
100 µm scaffold wall width	10.4	10.1	2.9
200 µm scaffold wall width	5.9	5.6	4.6

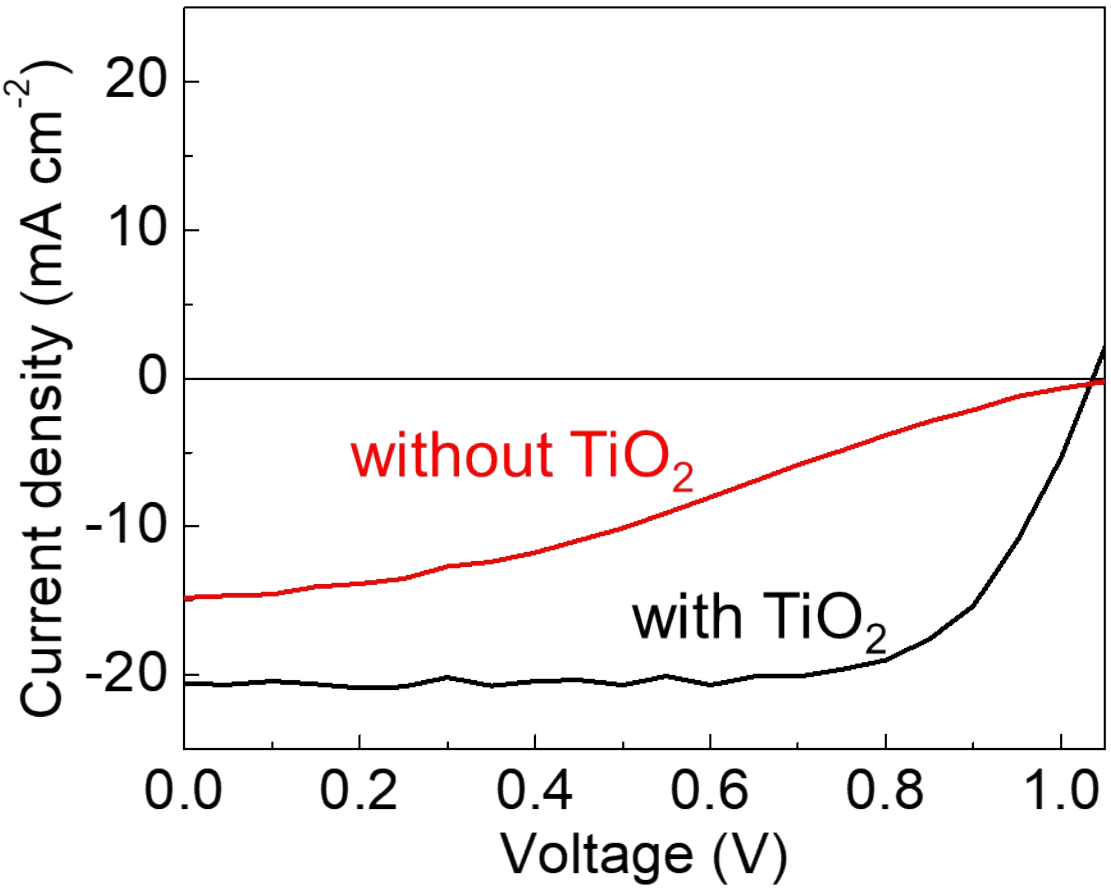

Figure S9. Devices fabricated with TiO_2 (ITO/TiO_2 NPs/C_{60}/$CH_3NH_3PbI_3$/PTAA/Ag) and without TiO_2 (ITO/C_{60}/$CH_3NH_3PbI_3$/PTAA/Ag), showing the importance of TiO_2 on device performance.

6. EQE of representative solar cells

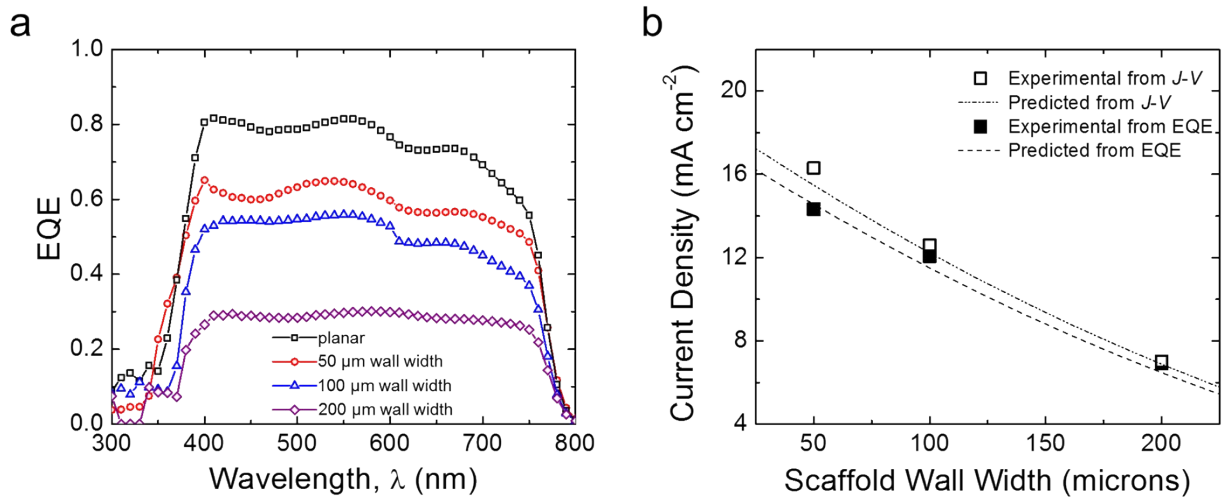

Figure S10. (a) External quantum efficiency (EQE) spectra of a planar device and the CSC devices. (b) The experimentally measured J_{sc}s based on these EQEs and the *J-V* curves for the different CSC scaffold wall widths. Predicted J_{sc}s were also calculated by multiplying the f_{MA} by the J_{sc}s measured for the planar device.

7. Accelerated aging- Damp heat test (ISOS D-3: 85 °C, 85% R.H.)

We performed aggressive stability measurements on encapsulated scaffold-partitioned CSC and planar perovskite solar cells. To completed devices, we soldered Ag ribbon to the electrode contacts and subsequently laminated them between two sheets of glass with the elastomeric polymer ethylene-vinyl acetate (EVA) (Specialized Technology Resources, Inc. Formulation 15585P/UF/HLT), which is the industrial standard for encapsulating c-Si modules. The EVA lamination was performed in a vacuum bag under house vacuum (Fibre Glast), 10 kPa pressure, and heat (120 °C for 10 min to melt the EVA and allow it to conformally bond to the cell, followed by 140 °C for 10 min to fully crosslink the EVA). A butyl rubber edge seal was applied to the perimeter of the glass and cured simultaneously with the EVA as an additional moisture barrier.

The packaged devices were then placed in an environmental chamber at 85 °C, 85% R.H. to adhere to the ISOS D-3 damp heat testing standards.(*1*) This accelerated test is a method for probing failure mechanisms much more quickly than would be observed under operational conditions. Aging devices for 1000 hours under these conditions is equivalent to a 10 year period of outdoor exposure in Miami, Florida. The normalized efficiency of two packaged devices over the course of 6 weeks (1008 hours) is shown in **Figure S9**, where the scaffold-partitioned device maintained 62% and planar device retained 47% of their initial efficiency values. This result shows CSC devices are capable of maintaining comparable or superior chemical stability to planar devices and can be successfully encapsulated to greatly slow undesirable chemical reactions.

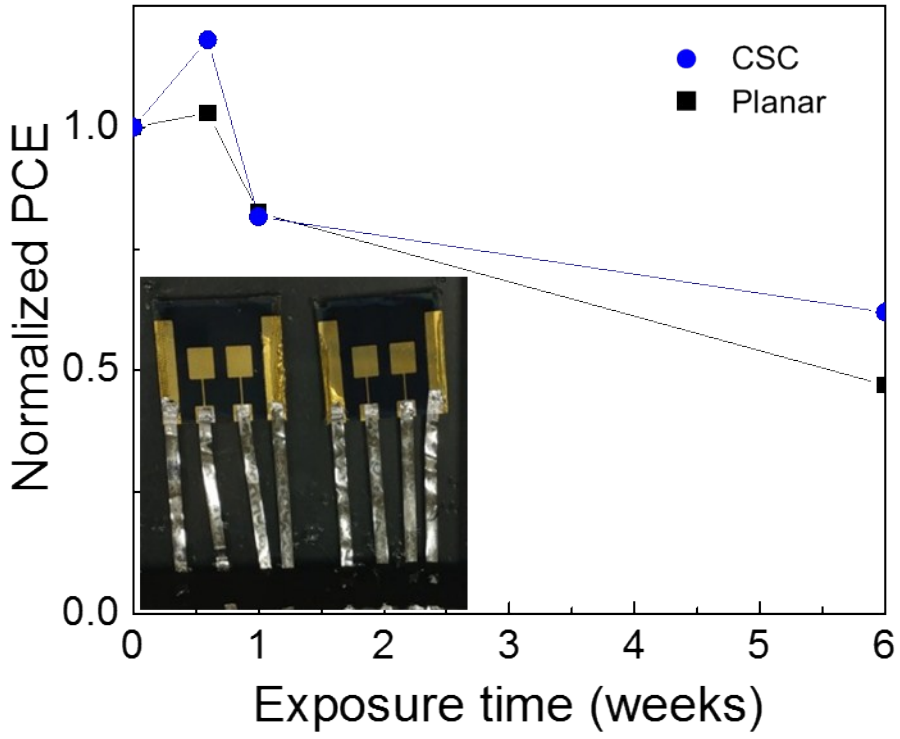

Figure S11. *J-V* curves under AM 1.5G illumination of scaffold-partitioned and planar perovskite devices after encapsulation and exposure to damp heat (85°C, 85% R.H.) up to 6 weeks. Inset: Photograph of encapsulated devices (planar on left, scaffold on right).

8. Photovoltaic response to increased light intensity

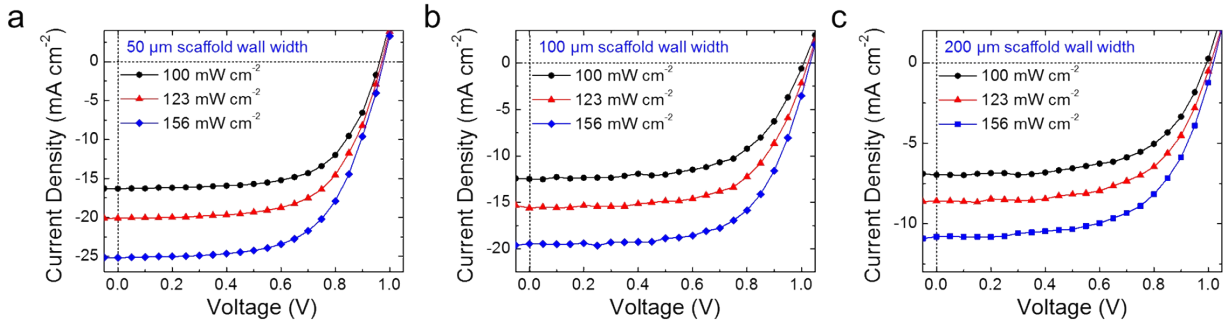

Figure S12. *J-V* curves of the CSC devices with different scaffold wall widths under different light intensities. Light intensities of 123 mW cm^{-2} and 156 mW cm^{-2} were selected because they represent the intensity of light assuming perfect photon management for the CSCs with 50 and 100 μm scaffold wall widths, respectively. A light intensity of 277 mW cm^{-2} (i.e., representative of the perfect photon management light intensity in 200 μm scaffold wall widths) was not tested due to lamp limitations.

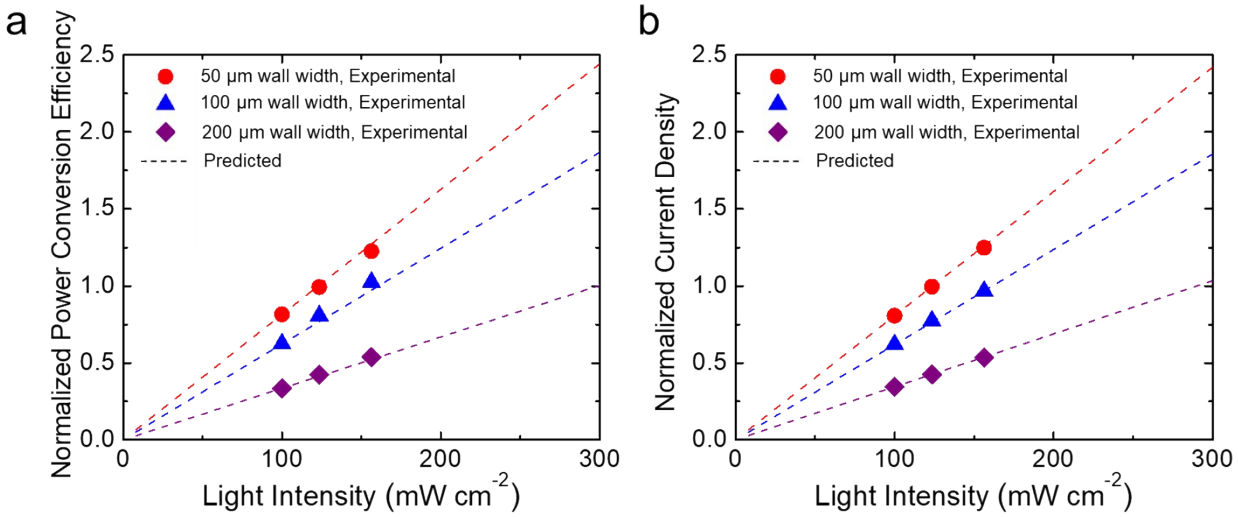

Figure S13. Photovoltaic characteristics of CSC devices with increasing light intensity. The devices were tested at three different light intensities, 100 mW cm^{-2}, 123 mW cm^{-2}, and 156 mW cm^{-2}. The normalized (a) *PCE* and the (b) J_{sc} of the CSC devices for all scaffold wall widths were plotted along with predicted normalized *PCE*s and J_{sc}s, which were calculated based on the device measurements at 100 mW cm^{-2}.

9. Experimental methods

9.1 Materials

ITO-coated glass slides (R_s ~ 10 Ω □$^{-1}$) were purchased from Xin Yan Technology. The $CH_3NH_3PbI_3$ precursors, methylammonium iodide (Dyesol) and lead acetate (Sigma Aldrich) were used as received. C_{60} was purchased from Materials and Electrochemical Research Corporation (MER Corp.). Poly(triarylamine) (PTAA) was purchased from Solaris. Positive photoresist, MEGAPOSIT™ SPR™ 3612, was purchased from Dow Electronic Materials and used as received. Anhydrous *N,N*-dimethylformamide (DMF) was purchased from Acros. EMD Millipore Extran® 300 (Fisher Scientific) was used as received. All other chemicals were purchased from Sigma Aldrich and used as received. TPBA was synthesized as reported elsewhere. (publication submitted)

9.2 Preparation of devices for cohesive fracture testing

Silicon wafers were diced into 3 cm × 3 cm coupons. Control specimens were fabricated by spin-coating a solution of methylammonium iodide (350.5 mg mL^{-1}) and lead acetate (278.8 mg mL^{-1}) in 940 μL DMF with a 60 μL additive of 1:100 hypophosphorous acid (HPA):DMF spin coated onto the beams at a speed of 2000 rpm for 75 s (after 15 s, N_2 was flowed into the spin-coater to improve film morphology). The resulting films were subsequently heated at 100 °C for 5 min in dry air to transition to the perovskite crystal structure.

Diced silicon coupons to be used to measure the fracture energy of the scaffold-partitioned perovskite layers were first placed in a Yield Engineering Systems (YES) oven operating at 150 °C and vapor-primed with hexamethyldisilazane (HMDS) to promote adhesion of the photoresist. A positive photoresist (SPR™ 3612) was subsequently spin-coated onto the beams at 5500 rpm for 30 s to form films ~1 μm thick (**Figure S2**). The residual solvent from the photoresist was removed with a pre-exposure bake on a hotplate at 90 °C for 60 s before the

specimens underwent UV exposure (365 nm, Karl Suss MA6) through the patterned photomask. Next, the specimens were developed in MF-26A until all residual exposed photoresist was removed, followed by a post-exposure hard bake on a hotplate at 115 °C for 60 s. The specimens were UV-ozone treated for 5 min to remove the HMDS on the surface of the substrate, and then further hard-baked on a hotplate at 200 °C for 20 min to improve the solvent resistance of the scaffold. The deposition of the perovskite into the scaffold was performed under the same conditions as described above. To act as a tough planarizing layer, a 15 mg mL^{-1} solution of PTAA—an organic hole-transporting semiconductor—and 4.5 mg mL^{-1} of 1,3,5,7-tetrakis-(*p*-benzylazide)-adamantane (TPBA)—an azide-modified adamantine cross-linker—in anhydrous toluene was spin-coated on top. The PTAA was then cross-linked by a 5 min exposure to UV-C light. An encapsulation layer of 5 nm of Cr and 100 nm of Al were evaporated onto the coupons before they were diced into 1.5 cm x 3 cm beams which were then sandwiched with E-20NS Loctite epoxy (cured at room temperature for 16 h in nitrogen) to a top silicon beam.

9.3 Cohesive fracture testing

Fracture testing of double cantilever beams (DCBs) was performed in laboratory air (~25 °C and ~40 % R.H.) under displacement control in a thin-film cohesion testing system (Delaminator DTS, Menlo Park, CA) which measured the load, P, versus displacement, Δ. The critical fracture energy, G_c (J m^{-2}), can then be calculated from equation 1:(*2*)

$$G_c = \frac{12P_c^2a^2}{b^2E'h^3}\left(1 + 0.64\frac{h}{a}\right)^2 \quad (1)$$

Where P_c is the critical load at which crack growth occurs, a is the crack length, E' is the plane-strain elastic modulus, and b and h are the width and half-thickness of the substrates,

respectively. The crack length, a, was estimated from the elastic compliance, $d\Delta/dP$, using the relationship in equation 2:

$$a = \left(\frac{d\Delta}{dP} \times \frac{bE^{'}h^{3}}{8}\right)^{1/3} - 0.64h \qquad (2)$$

Characterization of the fracture paths was performed by profilometry line scan (Veeco Dektak 150). The side of the beam containing the metal encapsulant is referred to as the ‘‘metal side’’ and the other side including the scaffold is referred to as the “scaffold side.” Compositional analysis of the chemical species at the surface of the fractured samples after DCB testing was performed with a survey X-ray photo spectroscopy (XPS, PHI 5000 Versaprobe) scan (0–1000 eV) using monochromatic Al Kα x-ray radiation at 1487 eV.

9.4 Preparation of photovoltaic devices

ITO-coated glass slides (2 cm × 2 cm) were cleaned with sequential ultrasonic baths (10 min each) in dilute Extran® 300 detergent solution, acetone, and then isopropanol before being dried with N_2 gas. Next, the ITO was coated with a 50 nm layer of TiO_2 nanoparticles (NPs) as follows. To one vial, 2.5 mL of anhydrous ethanol and 35 µL of 2 M HCl were added and stirred thoroughly. In another vial, 2.5 mL of anhydrous ethanol and 360 µL of titanium isopropoxide were added and stirred thoroughly. The solutions were then combined, stirred thoroughly, and filtered through a 0.2 µm PTFE filter, before being spin-coated on top of the ITO at 2000 rpm for 30 s to form a film 50 nm thick. The films were subsequently dried in air at 150 °C for 1 h. The scaffolds were then fabricated as described above.

A 15 nm thick layer of C_{60} was then thermally evaporated to fill pinholes in the TiO_2 NP film and improve its electron transport properties. The perovskite precursors were then spin-coated into the scaffold and heated as described above. A 15 mg mL^{-1} solution of PTAA—an

organic hole-transporting semiconductor—and 4.5 mg mL^{-1} of TPBA in anhydrous toluene with 10 µL mL^{-1} of 170 mg mL^{-1} Bis(trifluoromethane)sulfonamide lithium (LiTFSI) and 6 µL mL^{-1} of 4-tert-Butylpyridine (tBP) as dopants was then spin-coated on top of the perovskite at 4000 rpm for 45 s to form a layer 30 nm thick. The PTAA layer was then cross-linked. Next, the specimens were annealed on a hotplate at 75 °C for 5 min. Finally, the top electrode was added by evaporating a 150 nm thick layer of Ag through a shadow mask.

9.5 Photovoltaic device measurements

J-V curves were obtained using a Keithley 2400 digital source meter for devices under illumination with a flux of 100 mW cm^{-2} (or 123 mW cm^{-2} or 156 mW cm^{-2} for the CSCs measured with increased light intensity) from a 300 W xenon lamp AM 1.5 solar simulator (Oriel) which was calibrated by a KG5 photodiode. Active cells were masked to an area of 0.12 cm^2 and optimized with light soaking for optimal charge extraction and reduced trap states. The average figures of merit were calculated from the optimized conditions for each device and all reported curves were measured with a downward sweep at a rate of 0.1 s per step (0.05 V). Maximum power tracking was performed by using a perturb and measure program with steps of 5 mV to ensure stead-state photocurrent was reached.

9.6 Laser-beam induced current measurements

The LBIC scans for a planar perovskite solar cell and CSCs were performed similar to a manner previously described elsewhere.(*3*) Photocurrent maps were acquired using a custom-built LBIC system which was controlled by LabVIEW. A 0.7 mm continuous wave laser source (COHERENT OBIS LS 488 nm CW solid-state laser) was focused through a long working

distance infinity corrected 20x objective lens (Mitutoyo M Plan APO 20×/0.42) to produce a beam spot of ~35 μm in diameter, which was rastered across the cell. The intensity of the beam was controlled by using a neutral density filter (New Focus 5215) and optically chopped (Stanford Research Systems SR540 Optical chopper). Current was continuously monitored by connecting the anode and cathode of the solar cell to a transimpedance amplifier (Oriel). The signal was converted to voltage and sent to a lock0in amplifier (Stanford Research Systems SR830 DSP Lock-In Amplifier) for detection.

9.7 EQE measurements

External quantum efficiency (EQE) was recorded as a function of the wavelength using a Keithley model 236 source-measure unit. A 100 W tungsten bulb (Newport) was used as the excitation source and directed through a Princeton Instruments SpectraPro 150 monochromator. The monochromatic light was chopped at about 72 Hz and a pair of Stanford Research Systems SR830 lock-ins were used to monitor the perovskite signal at the chopping frequency. Data were averaged for 1 s at each wavelength with step sizes of 10 nm from 300 to 800 nm. No white-light or electrical bias was used during the EQE measurements of the perovskite solar cells.

10. References

1. M. O. Reese *et al.*, Consensus stability testing protocols for organic photovoltaic materials and devices. *Sol. Energy Mater. Sol. Cells*. **95**, 1253–1267 (2011).
2. M. F. Kanninen, An Augmented Double Cantilever Beam Model for Studying Crack Propagation and Arrest. *Int. J. Fract.* **9**, 83–91 (1973).
3. C. H. Peters *et al.*, High Efficiency Polymer Solar Cells with Long Operating Lifetimes. *Adv. Energy Mater.* **1**, 491–494 (2011).